Hybrid femtosecond/picosecond pure rotational anti-Stokes Raman spectroscopy of nitrogen at high pressures (1-70 atm) and temperatures (300-1000 K)

This manuscript was accepted by Appl. Phys. Lett. Click here to see the version of record.

Hybrid femtosecond/picosecond pure rotational anti-Stokes Raman spectroscopy of nitrogen at high pressures (1-70 atm) and temperatures (300-1000 K)

Trevor L. Courtney,[1] Nils Torge Mecker,[2] Brian D. Patterson,[1] Mark Linne,[2] and Christopher J. Kliewer[1,a)]

[1]*Combustion Research Facility, Sandia National Laboratories, Livermore, California 94551, USA*

[2]*School of Engineering, The University of Edinburgh, EH8 3JL Edinburgh, United Kingdom*

We demonstrate hybrid femtosecond/picosecond (fs/ps) pure-rotational coherent anti-Stokes Raman spectroscopy (RCARS) at high temperatures and pressures. Pulse-shaper-produced 40 fs pulses and bandwidth-narrowed, frequency-upconverted 5 ps pulses interact in a high-pressure cell containing N_2 at 1–70 atm and 300–1000 K. Accurate experimental temperatures evaluated from fits to model rotational spectra confirm that the sensitivity and precision advantages of hybrid fs/ps RCARS can be exploited in characterizing combustion environments, even in the pressure regime where significant collisional energy transfer and line broadening cannot be neglected.

Coherent anti-Stokes Raman spectroscopy (CARS) has been an important tool for temperature and species concentration measurements in gas-phase applications for years.[1-2] The CARS signal does not suffer from the background interference effects of incoherent techniques, and nanosecond or picosecond-pulse CARS has been widely used in the elevated temperature and pressure conditions of many combustion processes.[1] Vibrational CARS (VCARS) experiments of nitrogen (N_2) at ≤2500 atm reported on pressure-induced collisional effects and temperature models.[3-4] In VCARS, increased pressure causes the mixing of individual rovibrational lines and the eventual collapse of the rotational structure,[5] but the line spacing in pure-rotational CARS (RCARS) increases the pressure threshold for this collisional narrowing.[1,6] RCARS spectra of N_2 and O_2 exhibited pressure effects in studies up to 150 atm and various temperatures.[7-10]

More recently, hybrid femtosecond/picosecond (fs/ps) CARS techniques have been introduced, which can eliminate nonresonant signal and collisional dephasing of coherences as well as significantly reduce the single shot phase noise associated with broadband nanosecond dye lasers.[11-12] Hybrid fs/ps CARS benefits from high repetition rate, high peak power ultrafast lasers for efficient coherence excitation and improved accuracy and precision of CARS.[13] Furthermore, two-beam fs/ps CARS employs a single beam for pump/Stokes field interactions, which enables higher pulse energies and reduces the susceptibility to beam steering often present in turbulent combustion environments.[14] Only a few fs or fs/ps CARS experiments with moderate pressures

a) Author to whom correspondence should be addressed. Electronic mail: cjkliew@sandia.gov.

been published in the time domain at room temperature or in the frequency domain up to 900 K.[15-18] Recently, hybrid fs/ps vibrational CARS was demonstrated in flames up to 10 bar.[19] In this Letter, we present two-beam hybrid fs/ps RCARS at pressures up to 70 atm for temperatures up to 1000 K in a temperature- and pressure-controlled cell. We validate the capability to model the spectra in this regime where significant pressure-dependent line-broadening cannot be neglected.

The pulses used in the hybrid CARS experiment (Fig. 1) originate from the output of a Coherent Legend Elite Ti:Sapphire regenerative amplifier (795 nm, 1 kHz), which is seeded by a Coherent Vitara oscillator (100 MHz). The amplifier output is split into two beams of equal power, each of which is amplified in a single pass to ~9 mJ/pulse. One output beam provides the pump/Stokes pulses and passes through a grating compressor before a 35 μJ fraction of this 795 nm light enters a 4*f* pulse shaper (Femtojock) with a spatial light modulator (SLM) at the Fourier plane. Using the MIIPS algorithm,[20-21] we obtain a phase compensation mask to account for dispersion, including that from the thick gas cell entrance window. These windows exhibit both linear and nonlinear pulse dispersion, and the phase mask enables the production of a near transform-limited (TL) pulse at the experimental probe volume. Application of the phase mask to the SLM results in 42 fs TL pulses at the CARS interaction location, as determined by interferometric autocorrelation and frequency-resolved optical gating (FROG).[22-23]

To create the picosecond probe pulses from the other single-pass amplifier output beam, we frequency mix oppositely chirped pulses, adapting a technique developed by Raoult, et al.[24] This second-harmonic bandwidth compression (SHBC) method has been demonstrated previously in CARS. [25-26] In our setup, we split the strongly positively chirped (>100 ps) amplifier output between compressors with gratings equally but oppositely displaced from the grating separation required for pulse compression.[27] The chirped beams yield a probe centered at λ=397.5 nm via sum frequency generation (SFG) in a BBO crystal. The nearly TL pulses have full width at half maximum (FWHM) bandwidths, $\Delta\nu = 3.0$ cm^{-1}, after deconvolution with the separately measured 1.5 cm^{-1} spectrograph line spread function. Probe pulse durations of $\Delta t_{expt} \approx 5.5$ ps FWHM are measured via pump-probe intensity cross correlation of the nonresonant signal from argon. Additionally, the probe pulses pass through a folded 4*f* grating filter (f = 1 m, 1800 grooves/mm grating) to remove the following peripheral spectral components: 1.) blue-shifted satellite pulses that arise from interferences in the SFG of temporally chirped broadband pulses;[27] 2.) spectral wings due to imperfect conjugate chirping, i.e., frequency distributions in the fundamental pulses at each point in time. Filtering out the satellite pulses simplifies the CARS lineshapes. Elimination of the spectral wings, which are orders of magnitude weaker than the probe peak but comparable in strength to CARS signals, removes probe background noise in small-angle, two-beam CARS. Such filtering was not required in previous SHBC CARS experiments,[25-26] in which the SHBC beam and signal were not phase-matched collinearly.

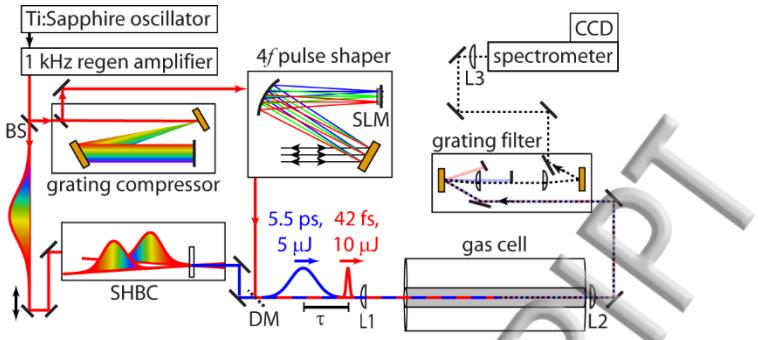

Fig. 1. Two-beam fs/ps CARS experiment with 1 kHz Ti:Sapphire laser system. Pump/Stokes pulses are grating compressed and dispersion compensated using a spatial light modulator (SLM) pulse shaper. Second-harmonic bandwidth compression (SHBC) probe pulses have a computer-controlled delay, τ. Vertically polarized beams are combined collinearly at a dichroic mirror (DM) and focused inside the gas cell. The grating-filtered CARS signal is focused into the spectrograph. Spherical lenses and focal lengths: L1, f = 300 mm; L2, f = 200 mm; L3, f = 75 mm.

The pump/Stokes and probe beams with matched vertical polarizations are routed to a gas cell for the CARS experiment. A computer-controlled translation stage (ThorLabs NRT100) provides the delay, τ, between the pulses. The beams are combined collinearly with a dichroic mirror and focused into a custom-built gas cell with an uncoated 300 mm focal length spherical lens. At their common focus, the 10 μJ/pulse pump/Stokes and 5 μJ/pulse probe beams have $1/e^2$ diameters of 100 μm and 70 μm, respectively. We use a collinear geometry in which beams (and signal) are normal to the cell windows to avoid spatial and temporal walkoff caused by refractive index changes of the 28-mm thick fused silica windows under pressure. This collinearity also lengthens the CARS interaction region (still <<200 mm enclosed cell length) for increased signal. The internal cell temperature profile is relatively flat along the beam propagation axis, as thermocouple readings over the central 120 mm (60 mm) are within 2% (0.5%) of the maximum temperature at the center of the cell. Pump/Stokes, probe, and signal beams are collimated in a 200 mm focal length lens after exiting the cell. For an economical, sharp-edge, spectral filter to isolate the CARS signal, we use the same 4f grating filter geometry as in the probe but with a single edge instead of a slit in the Fourier plane. The CARS signal is focused onto the entrance slit of a 0.550 m Czerny-Turner spectrometer (Horiba iHR550, 2400 grooves/mm grating) and spectrally dispersed onto a 400 × 1600 pixel (16 μm pixel size), back-illuminated CCD array (Andor DU971N-BV). The light is contained in an 11 x 1000 pixel region, which is vertically binned in <1 ms (10 μs exposure) to satisfy 1 kHz single-shot data collection.

This manuscript was accepted by Appl. Phys. Lett. Click here to see the version of record.

In this Letter, we perform N_2 RCARS at temperatures up to 1000 K and pressures up to 70 atm. Specifically, the stainless steel cell is rated for 1000 K up to 38 atm, after which pressure the maximum temperature decreases linearly to 293 K at 70 atm. The apparatus includes a preheater; however, the gas is typically sealed in the cell or kept at the minimum flow for maintaining pressure to match the cell gas temperature to that reported by the thermocouple in contact with the external cell wall. For each temperature and pressure combination, RCARS spectra are collected at a series of τ with steps of 1 ps centered at the first full revival of N_2 at ~8.4 ps, as determined by cross correlation in argon. In this range of delays, the nonresonant signal in N_2 is generally negligible compared to the resonant signal with pressure-dependent temporal decay. At each delay, 1000 laser shots are collected and averaged; the spectrum is background corrected and height normalized for fitting. In most cases, neutral density filters were placed in the probe beam to attenuate the signal as single laser shot signal levels were above the camera saturation threshold.

Aspects of the N_2 RCARS spectral modeling in this Letter are similar to those reported in previous fs/ps CARS studies.[12, 26, 28-29] The electric field of the near-TL probe pulse is included in the time-domain CARS model. We make two assumptions about the pump/Stokes pulse, which is not explicitly included in the model:[28] 1.) the pulse is TL, i.e., dispersion free; 2.) the pulse has infinite bandwidth (delta function in time). We impart the experimental spectral response on the model CARS spectra via multiplication by a pressure-specific nonresonant spectrum of argon. We avoid pulse overlap and nonresonant N_2 signal contributions with our choice of experimental τ. The molecular CARS response is represented by the time-dependent polarizability,

$$\chi(t) = i \sum_{\Delta J=+2} W_{JJ'} \sin\left(\omega_{JJ'} t\right) \exp\left[\left(-2\Gamma_J\right)t\right], \tag{1}$$

which is the sum of J to $J' = J + 2$ Stokes transition contributions (Figs. 2a,b, gray traces). Transitions between these angular-momentum quantum number defined states have frequencies, $\omega_{JJ'}$. Each linewidth, Γ_J, in Eq. (1) is the Lorentzian half-width at half maximum of the transition and is linearly dependent on pressure. To model collisional dephasing, and thus the frequency domain linewidths, we use the modified exponential gap (MEG) law for N_2,[30] including off-diagonal G-matrix terms to account for line-mixing effects at high pressures.[8, 16, 31] At the pressures of the experiments presented here, we do not observe significant changes in modeled RCARS N_2 spectra due to these off-diagonal elements. The $W_{JJ'}$ terms in Eq. (1) are weighting functions,

$$W_{JJ'} = \left(N_J - \frac{(2J+1)}{(2J'+1)} N_{J'} \right) b_{JJ'} F_J, \tag{2}$$

which include temperature-dependent rotational Boltzmann population distribution fractions, N_J; Placzek-Teller coefficients, $b_{JJ'}$; and Herman-Wallis factors, F_J.

The CARS time-domain electric field at τ is given as

$$\bar{E}_{CARS}(t-\tau) = \chi(t) E_{pr}(t-\tau) \exp[i\omega_0(t-\tau) - i\phi_{chirp}(t-\tau)^2/2], \quad (3)$$

the real component of which is shown in blue (red) in Fig. 2a (2b). In Eq.(3), E_{pr} is the electric field envelope of the probe with carrier frequency, ω_0. Following Yang, et al.,[26] we include the probe chirp in the RCARS model to improve the fitting of experimental data. The second-order phase term, ϕ_{chirp}, includes a scalar chirp factor, α,

$$\phi_{chirp} = \frac{d^2\phi}{dt^2} = 2\frac{(2\ln 2)\alpha}{\Delta t_{expt}^2}, \quad (4)$$

which provides a linear temporal chirp to account for the stretching of the probe pulse, $I_{pr} = E_{pr}^2$, beyond its Δν-dictated TL duration of $\Delta t_{expt}/\sqrt{1+\alpha^2}$.[26, 32] From the intensity cross correlation of experimental pulses, we determine Δt_{expt} of the probe from a single Gaussian fit to create ϕ_{chirp} (Figs. 2a,b, dotted black traces). The probe in these experiments has $\Delta t_{expt} \approx 5.5$ ps and $\Delta\nu = 3.0$ cm^{-1}, i.e., Δt_{expt} of I_{pr} is 12% longer than the TL duration. Given the dispersion $d\omega/dt = \phi_{chirp}$, the experimental α corresponds to $d\nu/dt = -0.25$ cm^{-1}/ps chirp. Removing the chirp contribution from Eq. (3) by setting $\alpha = 0$ causes the model spectra to have narrower transitions (corresponding to TL pulses of Δt_{expt} duration) and shifted transition frequencies compared to experimental spectra, depending on the magnitude and sign of α. Additionally, ϕ_{chirp} is responsible for observed subtler line-mixing and spectral wing characteristics in spectrally overlapping transitions, including those at high pressure. We found that a more careful determination of E_{pr} is necessary for accurate CARS spectra, so we modeled the temporal asymmetry of the probe by fitting the cross correlation to a sum of j Gaussians (typically $j = 2$),

$$E_{pr}(t-\tau) = \sum_j A_j \exp[-\frac{(2\ln 2)(t-\tau_j)^2}{t_j^2}], \quad (5)$$

This manuscript was accepted by Appl. Phys. Lett. Click here to see the version of record.

each with amplitude, A_j, and delay, τ_j (Fig. 2a,b, black traces, $j = 2$). A Fourier transform with respect to t of Eq. (3) yields the frequency-domain field. The square modulus is shifted by ω_0 to the CARS frequency axis and convolved with the spectrograph resolution function to give the model spectrum (Fig. 2c for two N_2 pressures).

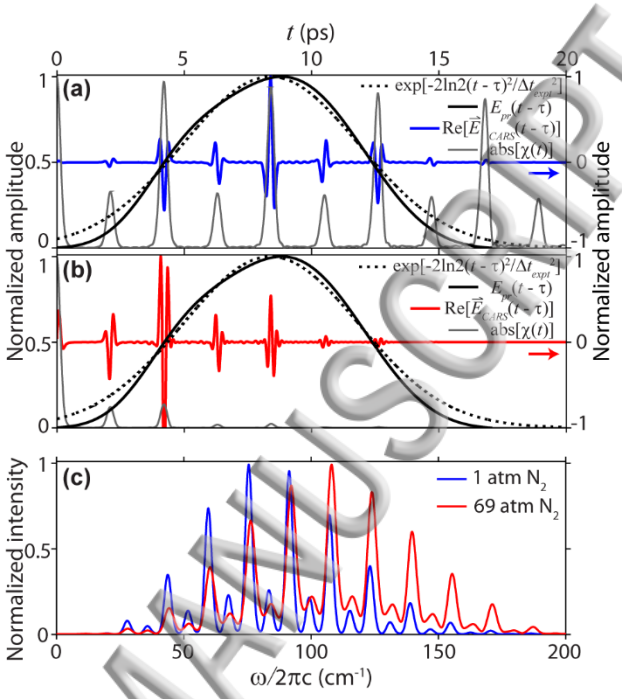

Fig. 2. RCARS model summary. (a,b) Modeled probe envelope as sum of two Gaussians (black trace) and as single Gaussian (dotted black trace). (a) CARS polarizability (gray trace) and electric field (blue trace) for 1 atm N_2. (b) CARS polarizability (gray trace) and electric field (red trace) for 69 atm N_2. (c) CARS spectra at 1 atm N_2 (blue trace) and 69 atm N_2 (red trace).

For comparison to a processed experimental spectrum, each simulated spectrum is cubic spline interpolated onto the calibrated experimental frequency axis and then multiplied by the nonresonant response. At a given temperature and pressure, parameters such as time delay and chirp are perfected beyond those obtained from the cross correlation by fitting the spectrum that is closest in τ to the first full revival of N_2, because of its simplicity and high resolution. Additionally, the more complicated and time-dependent envelopes of higher pressure spectra result in greater sensitivities to the choices of τ and α in the spectral models. In general, the delays τ and τ_j may be adjusted by ±0.2 ps, and the factor α by ±20%, from the cross correlation-determined values. Simulated spectra are combined in temperature libraries for nonlinear least-squares fitting of data in the spectral region of $J = 4$ through $20 < J < 30$, depending on temperature.

Six experimental N_2 spectra are shown in Fig. 3 (blue traces) along with best-fit models (red traces) and squared residuals (green traces). The first column has a room temperature, 7.8 atm N_2 spectrum (Fig. 3a), followed by an extreme case of each variable: 970 K and 7.8 atm (Fig. 3e), and 293 K and 69 atm (Fig. 3c). The 970 K spectrum displays the expected shift in population distribution with temperature. The blue shift of the 69 atm spectral envelope (Fig 3c) is dependent on τ and results from probing a strongly decaying coherence (Fig. 2b, gray trace). The mixing of the lines is evident, as the pressure is greater than the reported threshold of 6 MPa ≈ 59 atm for rotational line mixing.[7] The evaluated temperatures for spectra in this column are 286, 284, and 974 K, which differ by 2.4%, 3.1%, and 0.4% from the respective thermocouple readings of 293, 293, and 970 K.

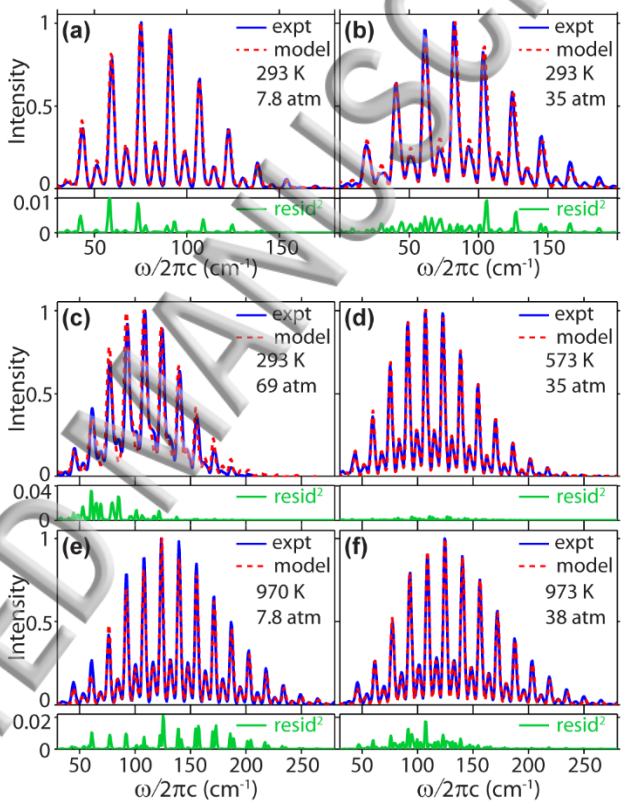

Fig. 3. Experimental and calculated RCARS spectra. Measured (blue traces) and best-fit temperature modeled (red traces) spectra are in top panels, and the squared (measured-modeled) residuals (green traces) are shown below the corresponding spectra. All the displayed spectra are recorded at a probe delay between 8 and 9 ps.

In the second column of Fig. 3, three spectra at different thermocouple-measured temperatures are shown for similar pressures (35-38 atm): 293 K (Fig. 3b), 573 K (Fig. 3d), and 973 K (Fig. 3f). All three display broadened linewidths compared to the spectra in Figs. 3a,e, but not yet broadened to the point of line mixing, as in Fig. 3c. Evaluated temperatures for spectra in this column are 280, 615, and 920 K, which differ from thermocouple readings by 4.4%, 7.3%, and 5.4%, respectively.

This work represents an extension of the hybrid fs/ps CARS technique into a pressure and temperature regime where collisional line-broadening cannot be neglected, even with the shortest duration probes that are yet capable of frequency resolving the signal. Such pressures and temperatures are important to many technologies, such as next-generation gas turbines and internal combustion engines, and viable *in-situ* diagnostic techniques are vitally important to technical progress in such systems. The instantaneous thermal field is a critical scalar for increased understanding of flame-wall interactions and thermal stratification in practical combustion systems. On a more fundamental level, diagnostics for probing high pressure and temperature systems will yield insight into such phenomena as three-body collisions and energy transfer in high pressure gas-phase chemical physics. While recent development has been devoted to exploiting the intrinsic benefit of hybrid fs/ps CARS of short probe time delays, which extends the pressure to which experiments may be performed in a nearly collision-free environment, there remains a large parameter space in pressure and temperature for which collisional effects and pressure-dependent line-mixing cannot be avoided. Here we show that the intrinsic benefits of hybrid fs/ps CARS, such as the removal of nonresonant contributions to the signal, higher precision and sensitivity, and the capability to use high-power kHz-rate fs lasers enabling higher data throughput rates, can be implemented in this pressure regime.

In conclusion, we report the development of a hybrid fs/ps RCARS experimental setup and accompanying model to collect accurate spectra in a high-pressure cell. The work in this Letter extends the reach of CARS temperature measurements in the simultaneously high temperature and pressure conditions that are typical in combustion environments. Performing these experiments in an optical engine in the future will provide an exciting test of the robustness of hybrid fs/ps RCARS for thermometry in a turbulent system.

SUPPLEMENTARY MATERIAL

See the supplementary material for an example of a dispersed CARS signal taken both with and without the pulse shaper mask applied to correct for nonlinear chirp components in the femtosecond pulse induced by the first cell window. Also included are sample FROG scan data taken after the high-pressure cell, demonstrating the improvement gained with the pulse shaper.

ACKNOWLEDGMENTS

This material is based upon work supported by an award from the United States Department of Energy's Office of Science Early Career Research Program, which supported the development of the CARS model, the laser equipment, and CJK. The construction of the high-pressure cell flow reactor, the femtosecond pulse shaper, and TLC were supported by the Laboratory

Directed Research and Development (LDRD) program at Sandia National Laboratories, which is a multimission laboratory managed and operated by National Technology and Engineering Solutions of Sandia, LLC., a wholly owned subsidiary of Honeywell International, Inc., for the U.S. Department of Energy's National Nuclear Security Administration under Contract DE-NA0003525. The views expressed in the article do not necessarily represent the views of the U.S. Department of Energy or the United States Government.

REFERENCES

1. A. C. Eckbreth, *Laser Diagnostics for Combustion Temperature and Species, Second Edition*. (Taylor & Francis, New York, 1996).
2. S. Roy, J. R. Gord, and A. K. Patnaik, Prog. Energy Combust. Sci. **36**, 280 (2010).
3. T. Bouche, T. Dreier, B. Lange, J. Wolfrum, E. U. Franck, and W. Schilling, Appl. Phys. B **50**, 527 (1990).
4. T. Dreier, G. Schiff, and A. A. Suvernev, J. Chem. Phys. **100**, 6275 (1994).
5. R. J. Hall, J. F. Verdieck, and A. C. Eckbreth, Opt. Commun. **35**, 69 (1980).
6. F. Vestin, D. Sedarsky, R. Collin, M. Alden, M. Linne, and P. E. Bengtsson, Combust Flame **154**, 143 (2008).
7. J. Bood, P. E. Bengtsson, and T. Dreier, J. Raman Spectrosc. **31**, 703 (2000).
8. G. Knopp, P. Beaud, P. Radi, M. Tulej, B. Bougie, D. Cannavo, and T. Gerber, J. Raman Spectrosc. **33**, 861 (2002).
9. T. Seeger, F. Beyrau, A. Brauer, and A. Leipertz, J. Raman Spectrosc. **34**, 932 (2003).
10. F. Vestin, M. Afzelius, H. Berger, F. Chaussard, R. Saint-Loup, and P. E. Bengtsson, J. Raman Spectrosc. **38**, 963 (2007).
11. B. D. Prince, A. Chakraborty, B. M. Prince, and H. U. Stauffer, J. Chem. Phys. **125**, 044502 (2006).
12. J. D. Miller, S. Roy, M. N. Slipchenko, J. R. Gord, and T. R. Meyer, Opt. Express **19**, 15627 (2011).
13. J. D. Miller, M. N. Slipchenko, T. R. Meyer, H. U. Stauffer, and J. R. Gord, Opt. Lett. **35**, 2430 (2010).
14. A. Bohlin, and C. J. Kliewer, J. Chem. Phys. **139**, 221101 (2013).
15. J. D. Miller, S. Roy, J. R. Gord, and T. R. Meyer, J. Chem. Phys. **135**, 201104 (2011).
16. P. J. Wrzesinski, H. U. Stauffer, W. D. Kulatilaka, J. R. Gord, and S. Roy, J. Raman Spectrosc. **44**, 1344 (2013).
17. G. Matthaus, S. Demmler, M. Lebugle, F. Kuster, J. Limpert, A. Tunnermann, S. Nolte, and R. Ackermann, Vib. Spectrosc. **85**, 128 (2016).
18. M. Kerstan, I. Makos, S. Nolte, A. Tunnermann, and R. Ackermann, Appl. Phys. Lett. **110**, 021116 (2017).
19. H. U. Stauffer, K. A. Rahman, M. N. Slipchenko, S. Roy, J. R. Gord, and T. R. Meyer, Opt Lett **43**, 4911 (2018).
20. V. V. Lozovoy, I. Pastirk, and M. Dantus, Opt. Lett. **29**, 775 (2004).

21. B. W. Xu, J. M. Gunn, J. M. Dela Cruz, V. V. Lozovoy, and M. Dantus, J. Opt. Soc. Am. B **23**, 750 (2006).
22. R. Trebino, K. W. DeLong, D. N. Fittinghoff, J. N. Sweetser, M. A. Krumbugel, B. A. Richman, and D. J. Kane, Rev. Sci. Instrum. **68**, 3277 (1997).
23. R. Trebino, and D. J. Kane, J. Opt. Soc. Am. A-Opt. Image Sci. Vis. **10**, 1101 (1993).
24. F. Raoult, A. C. L. Boscheron, D. Husson, C. Sauteret, A. Modena, V. Malka, F. Dorchies, and A. Migus, Opt. Lett. **23**, 1117 (1998).
25. S. P. Kearney, and D. J. Scoglietti, Opt. Lett. **38**, 833 (2013).
26. C. B. Yang, D. Escofet-Martin, D. Dunn-Rankin, Y. C. Chien, X. Yu, and S. Mukamel, J. Raman Spectrosc. **48**, 1881 (2017).
27. T. L. Courtney, N. T. Mecker, B. D. Patterson, M. Linne, and C. J. Kliewer, Opt Lett **44**, 835 (2019).
28. S. P. Kearney, D. J. Scoglietti, and C. J. Kliewer, Opt. Express **21**, 12327 (2013).
29. H. U. Stauffer, J. D. Miller, M. N. Slipchenko, T. R. Meyer, B. D. Prince, S. Roy, and J. R. Gord, J. Chem. Phys. **140**, 024316 (2014).
30. L. A. Rahn, and R. E. Palmer, J. Opt. Soc. Am. B **3**, 1164 (1986).
31. M. L. Koszykowski, R. L. Farrow, and R. E. Palmer, Opt. Lett. **10**, 478 (1985).
32. P. K. Upputuri, L. Gong, and H. F. Wang, Opt. Express **22**, 9611 (2014).

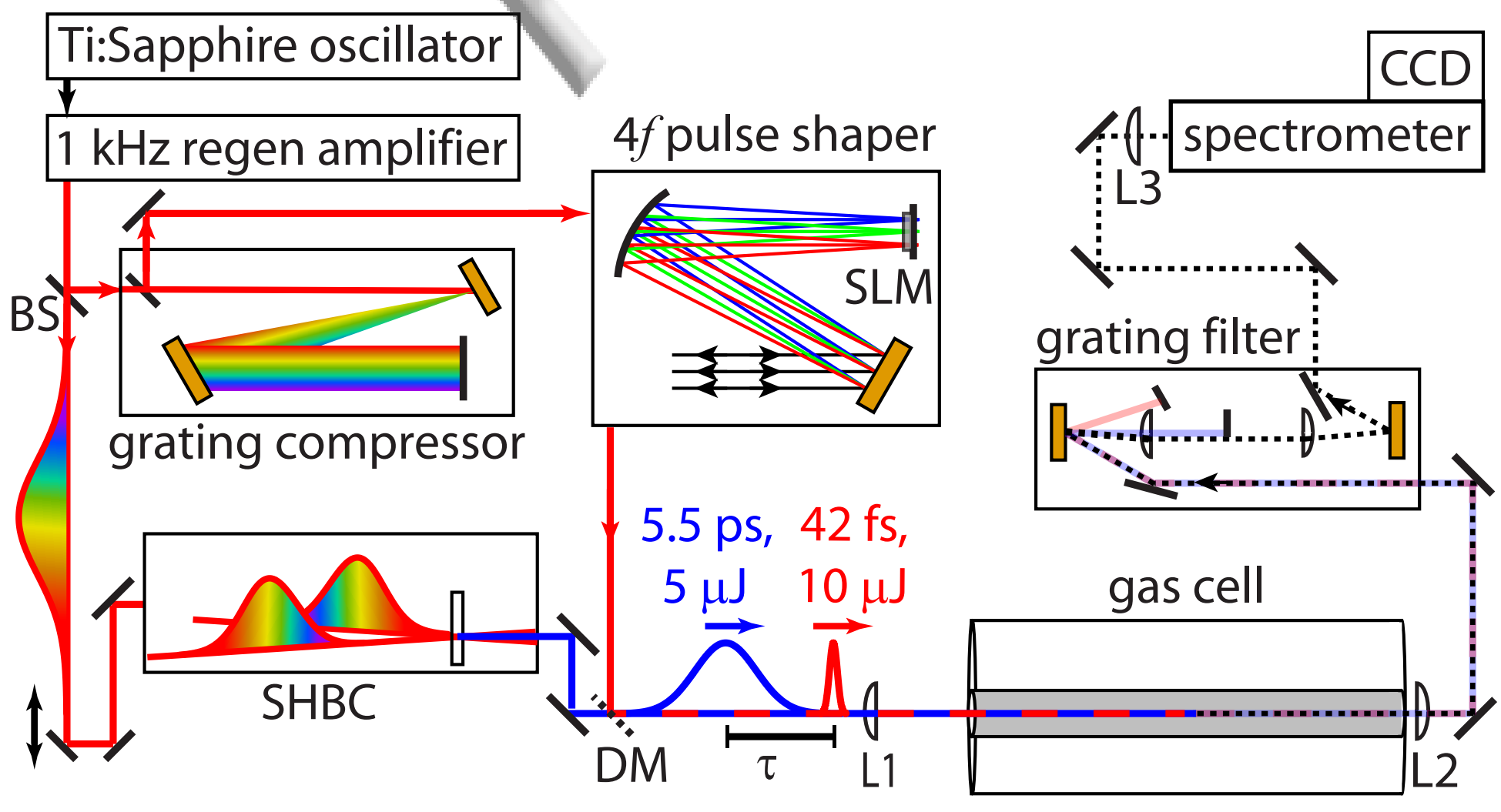
Ti:Sapphire oscillator
1 kHz regen amplifier
BS
grating compressor
4f pulse shaper
SLM
CCD
spectrometer
L3
grating filter
5.5 ps,
5 μJ
42 fs,
10 μJ
SHBC
gas cell
DM
τ
L1
L2

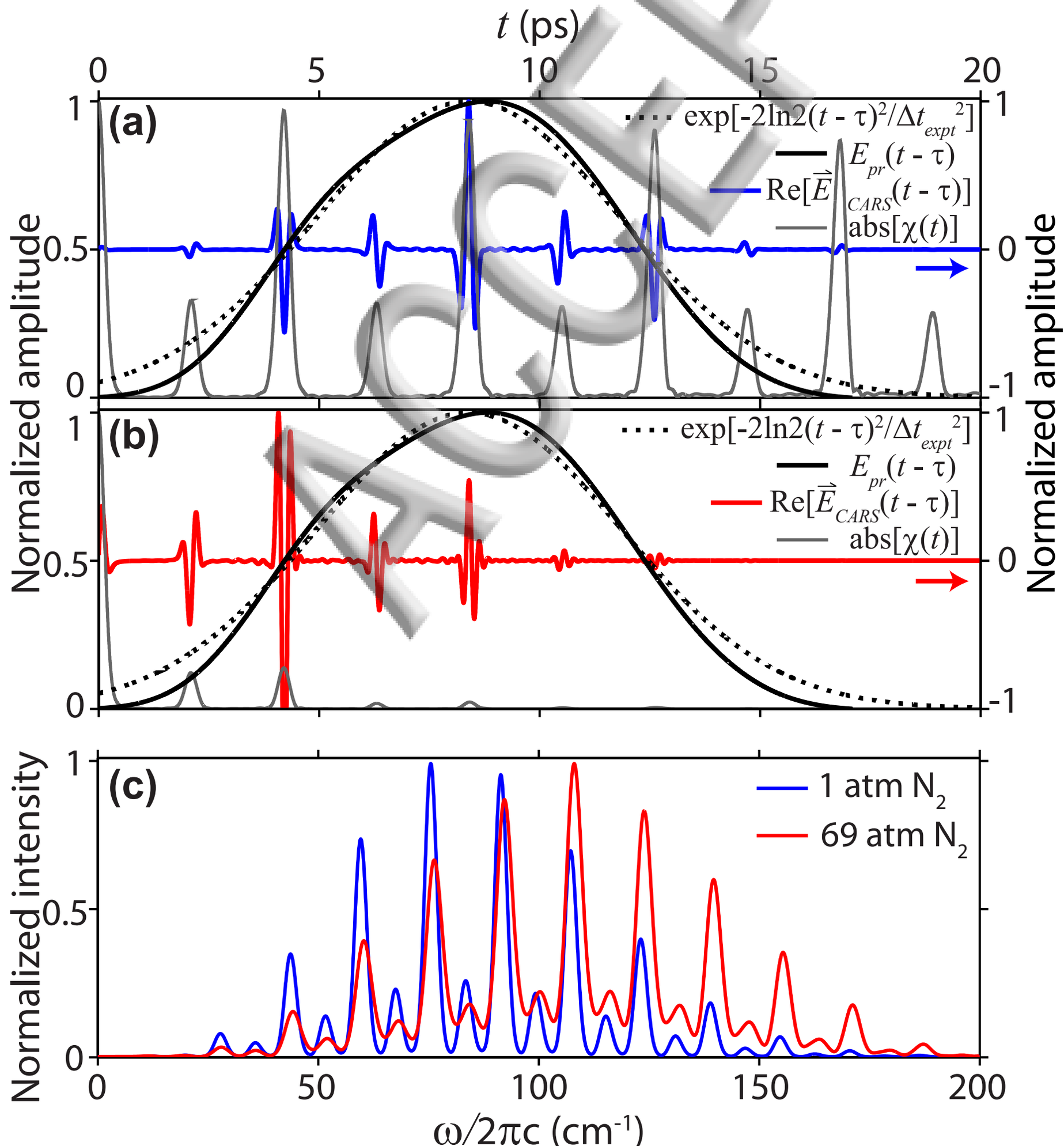
t (ps)
0
5
10
15
20
(a)
exp[-2ln2(t - τ)²/Δt_expt²]
E_pr(t - τ)
Re[Ẽ_CARS(t - τ)]
abs[χ(t)]
(b)
exp[-2ln2(t - τ)²/Δt_expt²]
E_pr(t - τ)
Re[Ẽ_CARS(t - τ)]
abs[χ(t)]
Normalized amplitude
Normalized amplitude
1
0.5
0
1
0
-1
(c)
1 atm N2
69 atm N2
Normalized intensity
1
0.5
0
0
50
100
150
200
ω/2πc (cm⁻¹)